Atomic structure of Mn-rich nanocolumns probed by x-ray absorption spectroscopy

M. Rovezzi,[1] T. Devillers,[2] E. Arras,[2] F. d'Acapito,[1] A. Barski,[2] M. Jamet,[2] and P. Pochet[2,a)]
[1]*CNR-INFM-OGG GILDA CRG c/o ESRF 6 Rue Jules Horowitz F-38043 Grenoble, France*
[2]*CEA, INAC, SP2M, F-38054, Grenoble, France*

(Received 28 April 2008; accepted 1 June 2008; published online 20 June 2008)

In this letter, we have used the extended x-ray-absorption fine-structure (EXAFS) technique to investigate the structure of Mn-rich self-organized nanocolumns grown by low temperature molecular beam epitaxy. The EXAFS analysis has shown that Mn-rich nanocolumns exhibit a complex local structure that cannot be described by a simple substitutional model. Additional interatomic distances had to be considered in the EXAFS model which are in excellent agreement with the structure of a Ge–3Mn building block tetrahedron of Ge_3Mn_5. © *2008 American Institute of Physics*. [DOI: 10.1063/1.2949077]

Intense efforts have recently been devoted to the fabrication of high Curie-temperature (T_C) ferromagnetic semiconductors for their potential incorporation into spintronic devices.[1] Among them, (Ge,Mn) seems to be a promising candidate due to its compatibility with mainstream silicon technology.[2] However, manganese dilution in a germanium crystal remains highly questionable and in most experiments (Ge,Mn) films contain either nanoscale Mn-rich regions or secondary phase precipitates such as Ge_3Mn_5. In the last case, Ge_3Mn_5 metallic inclusions prevent any spintronic applications[3] whereas the intermediate regime, leading to the formation of transition metal rich regions, seems to be one possible means to raise, at least locally, the Curie temperature. This kind of regions have been already observed by other groups in (Ge,Mn),[4–6] (Zn,Cr)Te,[7] or (Ga,Mn)N.[8] In (Ge,Mn) these metal rich regions have the form of nanocolumns and a possible explanation for their formation is given in Ref. 9. While Mn atoms deposited at 150 K on a Ge(001) surface are trapped in subsurface interstitial sites, Mn monomers deposited at room temperature diffuse at the germanium surface to nucleate Mn-rich clusters leading to nanocolumns when increasing the film thickness. In (Zn,Cr)Te and (Ga,Mn)N, experimental observations could be qualitatively reproduced by numerical simulations in the spinodal decomposition framework.[10] In the present letter we focus on Mn-rich (>30%) nanocolumns that spontaneously self-assemble during the layer-by-layer growth of thin (Ge,Mn) films. Despite the high Mn concentration, nanocolumns still exhibit a diamond-like crystalline structure as derived from x-ray diffraction or high resolution transmission electron microscopy. They exhibit ferromagnetism up to 400 K. However, they are metastable nano-objects in the sense that annealing the samples leads to Ge_3Mn_5 precipitates which is the most stable (Ge,Mn) alloy. Nanocolumns could be stabilized in the Ge matrix using low temperature molecular-beam epitaxy (MBE) which is an out-of-equilibrium growth technique.[4] In this contribution, we will address the issue of the local environment of Mn in the nanocolumns using the extended x-ray absorption fine-structure (EXAFS) technique.[11]

$Ge_{1-x}Mn_x$ films were grown using solid sources MBE by codepositing Ge and Mn evaporated from standard Knudsen effusion cells on Ge(001) substrates. The sample investigated in this letter consist of 80 nm thick layer grown at 130 °C and contains 6% of Mn, GeMn(6%) in the following. The layer-by-layer growth mode as observed by reflection high-energy electron diffraction favors the formation of Mn-rich nanocolumns. Their diameter is 3 nm and composition close to Ge_2Mn. Details on structural and magnetic properties can be found in Ref. 4. In addition, two reference compounds have been grown: a diluted sample with 0.1% of Mn grown in the same conditions, GeMn(0.1%), and a 50-nm-thick Ge_3Mn_5 monocrystalline film grown on Ge(111) (62.5% Mn), Ge_3Mn_5. EXAFS measurements at the Mn *K* edge (6539 eV) have been carried out at the "GILDA" Italian Collaborating Research Group beamline at the European Synchrotron Radiation Facility in Grenoble.[12] Details on the experimental setup can be found in the experimental section of Ref. 13.

The quantitative analysis has been done with the IFEFFIT/ATHENA/ARTEMIS programs[14,15] using the atomic models described below. Theoretical EXAFS signals were computed with the FEFF8 code[16] using muffin tin potentials and the Hedin–Lunqvist approximation for their energy-dependent part. EXAFS data and the best fits for the samples described before are reported in Fig. 1 and Table I. All the fits were carried out in the Fourier-transformed space (*R* space) from the *k*-weighted EXAFS data and the variable parameters were: ΔE_0 (the refinement of the edge position) and N_i, R_i, σ_i^2, respectively, the coordination number, the interatomic distance and the Debye–Waller factor, for the i^{th} atomic shell around Mn. Looking at the EXAFS spectra in Fig. 1, the main differences between the samples lie in the low-*k* range between 3 and 4 $Å^{-1}$ at two peak positions labelled peak 1 and peak 2 (vertical dashed lines in Fig. 1): the diluted film exhibits peak 1, Ge_3Mn_5 exhibits peak 2 and only ferromagnetic nanocolumns exhibit both peaks which may be the fingerprint of this system. In addition, the Fourier transform (Fig. 1, right) shows only a single dominant peak with no evidence of the second and third coordination shell of the tetrahedral structure as instead present in (Ga,Mn)As.[13] This is a typical effect of local structural disorder as encountered in amorphous Ge.[17] For this reason

a)Electronic mail: pascal.pochet@cea.fr.

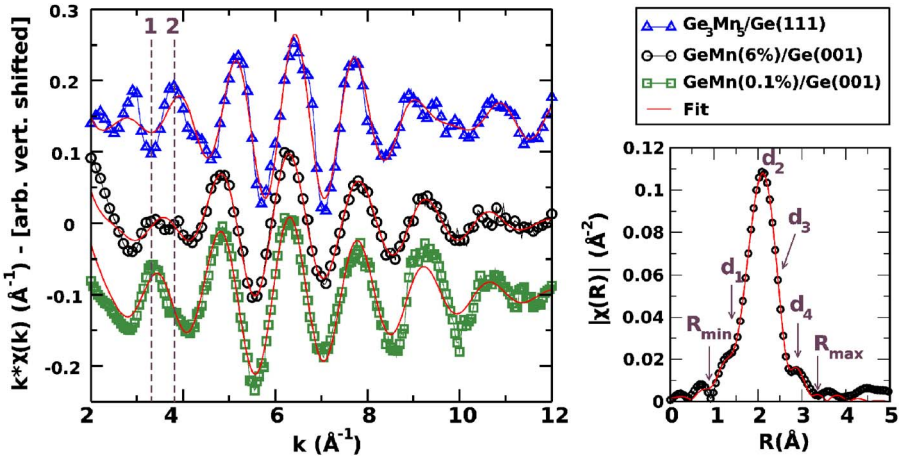

FIG. 1. (Color online) Left: *k*-weighted EXAFS spectra of the different samples. Right: Fourier transform for the sample GeMn(6%) calculated in the *k*-range 3–10 Å^{-1} using a Hanning window (Ref. 18). The fits have been performed in *R* space in the range from R_{min}=1.0 Å to R_{max} =3.35 Å. For all scattering paths a common amplitude parameter S_0^2 has been fixed to a value of 0.935, as computed for this material by the FEFF8 code using a full-multiple-scattering calculation.

only the first coordination shell analysis is possible, constructing a theoretical model based on the informations obtained from the two model compounds in order to reduce correlations between variables used in the fits. The diluted film, GeMn(0.1%), is correctly reproduced using a single atomic shell, representing Mn in a substitutional Ge site with a distance d_2 and coordination number N_2 (see Table I); the fitted Debye–Waller factor, $\sigma_2^2=0.012\pm0.003$ Å^2, is quite high and denotes a substitutional defect with a strong local disorder. In the same way, the EXAFS data of the Ge_3Mn_5 film could be reproduced[19] with the theoretical distances (d_2, d_3, and d_4) and coordination number extracted from perfect Ge_3Mn_5 hexagonal $D8_8$ structure.[20]

A single substitutional defect at a distance d_2 could not account for the EXAFS oscillations of ferromagnetic nanocolumns in the low-*k* range. For this reason we added distances d_3 and d_4 to the model as in Ge_3Mn_5, obtaining an improvement of the fit in the high *R* part of the main peak in the Fourier transform. Note that, for these bonds, we could not make a difference between Ge and Mn backscatterers. The EXAFS oscillations for distances d_3 and d_4 are in antiphase with the oscillations of distance d_2 leading to the appearance of both peaks 1 and 2 in the low-*k* region. Finally, the addition of a fourth shorter scattering path at a Mn–Mn distance d_1 permitted to improve the fit. In order to reduce correlations between variables, the Debye–Waller factors for distances d_1, d_3, and d_4 have been set equal to the value found for distance d_2 (0.013 ± 0.001 Å^2). Noteworthy, other possibilities, such as an oxide contribution, were also explored and resulted not to improve the agreement with experiment. We underline that each time an additional scattering path was added in the fit, its effectiveness was verified by a χ^2 test.

The stability of substitutional Mn in diluted GeMn and Mn–Mn short bonds is consistent with *ab initio* calculations[21,22] and Mn–Mn dimers have been already observed in experimental EXAFS studies of Mn in InAs[23] and in Ge.[24] It is worth noting that despite the complex hexagonal structure of Ge_3Mn_5, Mn–Mn and Mn–Ge distances[20] in this compound are comparable within error bars to the three experimental lengths d_2, d_3, and d_4 respectively. The main difference arises from the coordination number of distance d_4 which is much higher in the case of Ge_3Mn_5. This difference can be assigned to the presence of two sites for Mn atoms in the Ge_3Mn_5 structure (see Fig. 2). The Ge_3Mn_5 structure can be described using two kinds of Ge–3Mn tetrahedra. However, only the tetrahedron that just contains Mn atoms in site 2 (Mn2, the orange tetrahedron in Fig. 2) fits with the local structure parameters experimentally found in the Mn-rich nanocolumns sample. Therefore we can assume that Mn-rich nanocolumns are mostly made of these Ge–3Mn tetrahedra that contains only Mn2 atoms, the short Mn–Mn bonds being in the Ge matrix. In fact, almost 90% of the Mn is within the nanocolumns and the 10% Mn present in the matrix is expected to be poorly visible. Indeed in GeMn(6%) the d_2 distance involves a Ge backscatterer at 2.49 ± 0.01 Å that is larger than the d_2 distance in GeMn(0.1%), 2.47 ± 0.01 Å, and approaches the Ge–Mn2 distance d_2 in the orange tetrahedron (Fig. 2) of hexagonal Ge_3Mn_5 (2.482 Å). Structural similarities between Mn-rich nanostructures embedded in a germanium matrix and Ge_3Mn_5 have already been proposed.[24,25] The agreement arises from the common Ge–3Mn tetrahedron found in both structures. These tetrahedra are indeed building blocks of Ge_3Mn_5 as well as nanocolumns. Nevertheless, we believe that the formation of these Ge_3Mn_5 building blocks is induced by the low tem-

TABLE I. Results of the EXAFS analysis: interatomic distances, coordination numbers, and corresponding backscatterers are reported. Distance labels are consistent with the EXAFS analysis: d_1 stands for the short Mn–Mn distance, d_2 stands for the first nearest neighbor distance in Ge or for the average of the short distance in the Ge_3Mn_5 tetrahedra, while d_3 and d_4 stand for the two longer distances in the tetrahedra (see Fig. 2).

	Distance (Å)—Coordination							
	d_1		d_2		d_3		d_4	
Sample	±0.02	±0.1	±0.01	±0.5	±0.05	±0.4	±0.05	±0.5
GeMn(0.1%)	-	-	2.47	4.2[a]	-	-	-	-
GeMn(6%)	2.11	0.2[b]	2.49	4.0[a]	2.86	1.2[c]	3.10	1.3[c]
Ge_3Mn_5	-	-	2.52	5.0[d]	2.70	1.2[a]	3.04	8.4[b]

[a]Ge backscatterer.
[b]Mn backscatterer.
[c]Ge or Mn backscatterer.
[d]Ge and Mn backscatterer.

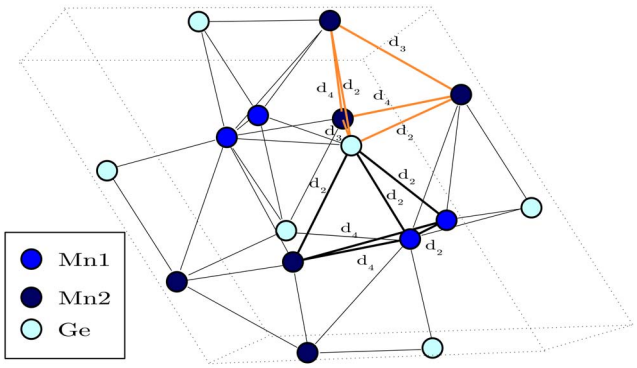

FIG. 2. (Color online) Perspective view of the unit cell of Ge_3Mn_5. Colored spheres denote Ge (cyan) and the two types of Mn atoms,[20] Mn1 (blue) and Mn2 (dark blue). The black Ge–3Mn tetrahedron, that contains both Mn1 and Mn2 atoms, exhibits d_2 and d_4 distances including Mn and Ge backscatterers for the d_2 distance. The orange Ge–3Mn tetrahedron, that contains only Mn2 atoms, exhibits d_2, d_3 and d_4 distances and only Mn–Ge bonds at d_2.

perature used during the MBE growth. Moreover we can suggest that the high-T_C ferromagnetism properties of Mn-rich nanocolumns might be connected to the long Mn–Mn distance within this tetrahedron (d_3 and d_4) as proposed by Forsyth and Brown to explain the magnetic structure of Ge_3Mn_5.[20] The absence of the d_2 Mn–Mn distance (only present between Mn1-type atoms) could explain the high magnetization found in the Mn-rich nanocolumns sample.[4] However this interpretation has to be investigated in more detail in the future. Indeed, using different growth conditions (Mn concentration and growth temperature) we could recently evidence Mn-rich nanocolumns exhibiting different magnetic properties while keeping their diamond-like crystalline structure.[26] This demonstrates that Mn concentration and position in the nanocolumns is highly sensitive to growth conditions on Ge(001) and fully determines magnetic properties; thus a detailed description of the local environment around Mn is mandatory to fully understand the magnetic properties.

To summarize, we have used EXAFS measurements to investigate the local structure of Mn-rich nanocolumns grown by low temperature MBE. The EXAFS analysis has shown that Mn-rich nanocolumns present complex local structure that cannot be described only with a simple substitutional model. Additional interatomic distances have to be considered in EXAFS analysis which are in good qualitative and quantitative agreement with the structure of one of the Ge–3Mn building block tetrahedron found in Ge_3Mn_5 crystal. The formation of such tetrahedra in Mn-rich nanocolumns should be allowed due to the low temperature MBE growth. Finally we suggest that the high-T_C ferromagnetism properties of the MBE films may originate from this local order found in both GeMn nanocolumns and Ge_3Mn_5.

We acknowledge the European Synchrotron Radiation Facility and the Italian Collaborative Research Group for provision of synchrotron radiation facilities. GILDA is a project jointly financed by CNR and INFN.

[1] I. Zutic, J. Fabian, and S. D. Sarma, Rev. Mod. Phys. **76**, 323 (2004).
[2] Y. D. Park, A. T. Hanbicki, S. C. Erwin, C. S. Hellberg, J. M. Sullivan, J. E. Mattson, T. F. Ambrose, A. Wilson, G. Spanos, and B. T. Jonker, Science **295**, 651 (2002).
[3] Y. D. Park, A. Wilson, A. T. Hanbicki, J. E. Mattson, T. Ambrose, G. Spanos, and B. T. Jonker, Appl. Phys. Lett. **78**, 2739 (2001).
[4] M. Jamet, A. Barski, T. Devillers, V. Poydenot, R. Dujardin, P. Bayle-Guillemaud, J. Rothman, E. Bellet-Amalric, A. Marty, J. Cibert, R. Mattana, and S. Tatarenko, Nat. Mater. **5**, 653 (2006).
[5] D. Bougeard, S. Ahlers, A. Trampert, N. Sircar, and G. Abstreiter, Phys. Rev. Lett. **97**, 237202 (2006).
[6] A. P. Li, C. Zeng, K. van Benthem, M. F. Chisholm, J. Shen, S. V. S. Nageswara Rao, S. K. Dixit, L. C. Feldman, A. G. Petukhov, M. Foygel, and H. H. Weitering, Phys. Rev. B **75**, 201201(R) (2007).
[7] S. Kuroda, N. Nishizawa, K. Takita, M. Mitome, Y. Bando, K. Osuch, and T. Dietl, Nat. Mater. **6**, 440 (2007).
[8] M. Moreno, A. Trampert, B. Jenichen, L. Däweritz, and K. H. Ploog, J. Appl. Phys. **92**, 4672 (2002).
[9] C. Zeng, Z. Zhang, K. van Benthem, M. F. Chisholm, and H. H. Weitering, Phys. Rev. Lett. **100**, 066101 (2008).
[10] T. Fukushima, K. Sato, H. Katayama-Yoshida, and P. H. Dederichs, Jpn. J. Appl. Phys., Part 2 **45**, L416 (2006).
[11] P. A. Lee, P. H. Citrin, P. Eisenberger, and B. M. Kincaid, Rev. Mod. Phys. **53**, 769 (1981).
[12] F. d'Acapito, S. Colonna, S. Pascarelli, G. Antonioli, A. Balerna, A. Bazzini, F. Boscherini, F. Campolungo, G. Chini, G. Dalba, G. I. Davoli, P. Fornasini, R. Graziola, G. Licheri, C. Meneghini, F. Rocca, L. Sangiorgio, V. Sciarra, V. Tullio, and S. Mobilio, ESRF Newsl. **30**, 42 (1998).
[13] F. d'Acapito, G. Smolentsev, F. Boscherini, M. Piccin, G. Bais, S. Rubini, F. Martelli, and A. Franciosi, Phys. Rev. B **73**, 035314 (2006).
[14] B. Ravel and M. Newville, J. Synchrotron Radiat. **12**, 537 (2005).
[15] M. Newville, J. Synchrotron Radiat. **8**, 322 (2001).
[16] A. L. Ankudinov, B. Ravel, J. J. Rehr, and S. D. Conradson, Phys. Rev. B **58**, 7565 (1998).
[17] F. Evangelisti, M. G. Proietti, A. Balzarotti, F. Comin, L. Incoccia, and S. Mobilio, Solid State Commun. **37**, 413 (1981).
[18] The limited k range in the analysis is due to noise and distortions in the fluorescence EXAFS spectra introduced by the system itself. In fact, the presence of a crystalline substrate and a buffer layer induces Bragg reflections and standing-wave enhanced fluorescence that is impossible to completely remove in our experimental conditions.
[19] The fit of 50 nm thick Ge_3Mn_5 film grown on Ge(111) was performed only for the first coordination shell because complex multiple scattering paths should be included for higher coordination shells and single scattering paths were recalculated for averaged distances d_2, d_3, and d_4. Debye–Waller factors are, respectively, $\sigma_2^2=0.003\pm0.001$ Å^2, $\sigma_3^2=0.003\pm0.001$ Å^2, and $\sigma_4^2=0.004\pm0.001$ Å^2.
[20] J. B. Forsyth and P. J. Brown, J. Phys.: Condens. Matter **2**, 2713 (1990).
[21] A. J. R. da Silva, A. Fazzio, and A. Antonelli, Phys. Rev. B **70**, 193205 (2004).
[22] A. Continenza, G. Profeta, and S. Picozzi, Phys. Rev. B **73**, 035212 (2006).
[23] Y. L. Soo, S. Kim, Y. H. Kao, A. J. Blattner, B. W. Wessels, S. Khalid, C. S. Hanke, and C.-C. Kao, Appl. Phys. Lett. **84**, 481 (2004).
[24] L. Ottaviano, M. Passacantando, A. Verna, R. Gunnella, E. Principi, A. D. Cicco, G. Impellizzeri, and F. Priolo, J. Appl. Phys. **100**, 063528 (2006).
[25] S.-K. Kim, Y. C. Cho, S.-Y. Jeong, C.-R. Cho, S. E. Park, J. H. Lee, J.-P. Kim, Y. C. Kim, and H. W. Choi, Appl. Phys. Lett. **90**, 192505 (2007).
[26] T. Devillers, M. Jamet, A. Barski, V. Poydenot, P. Bayle-Guillemaud, E. Bellet-Amalric, S. Cherifi, and J. Cibert, Phys. Rev. B **76**, 205306 (2007).